Preprint of: Kozicki J., Jasik P., Kilich T., Sienkiewicz J., Optimization of the femtosecond laser impulse for excitation and the Spin-Orbit mediated dissociation in the NaRb Dimer, JOURNAL OF QUANTITATIVE SPECTROSCOPY & RADIATIVE TRANSFER Vol. 306, (2023), 108644, DOI: 10.1016/j.jqsrt.2023.108644

Optimization of the Femtosecond Laser Impulse for Excitation and the Spin-Orbit Mediated Dissociation in the NaRb Dimer

J. Kozicki[a,b], P. Jasik[a,c,*], T. Kilich[a,b], J. E. Sienkiewicz[a,b]

[a] *Faculty of Applied Physics and Mathematics, Gdańsk University of Technology, 80-233 Gdańsk, Poland*
[b] *Advanced Materials Center, Gdańsk University of Technology, 80-233 Gdańsk, Poland*
[c] *BioTechMed Center, Gdańsk University of Technology, 80-233 Gdańsk, Poland*

Abstract

We study the dynamics of multiple coupled states under the influence of an arbitrary time-dependent external field to investigate the femtosecond laser-driven excitation and the spin-orbit mediated dissociation in the NaRb dimer. In this process, the dimer is excited from the ground triplet state $1^3\Sigma^+$ to the $1^3\Pi$ state using the femtosecond laser impulse and the spin-orbit coupling between the $1^3\Pi$ and $2^1\Sigma^+$ states results in the singlet-triplet transition. The laser impulse parameters are optimised to obtain maximum yield in electronic states correlating with the first excited atomic asymptote. We observe the detailed population statistics and power-law decay of these states. Finally, the analysis of the population oscillations allows us to determine the optimal time delay for dumping the molecule to its absolute ground state.

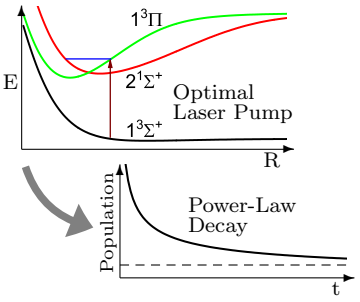

Graphical Abstract

1. Introduction

Quantum dynamics is a growing discipline at the interface of chemistry, physics and materials science [1]. It allows studying the behaviour of objects in a way, that emphasizes the quantum nature of their evolution in time. Quantum dynamics simulations are an indispensable tool for investigating processes such as chemical reactions [2], field-molecule interactions [3] and quantum computing [4, 5]. The particular emphasis is placed on investigating the photoinduced dynamics of breaking (dissociation) [6, 7, 8, 9, 10, 11] and creating (association) [12, 13, 14, 15, 16, 17] of the chemical bonds in the molecular systems. Photoassociation processes play a key role in the field of cold and ultracold physics and chemistry, allowing for the formation of molecules in the deeply bound ground states and investigation of their unique quantum properties [18, 19, 20, 21, 22]. On the other side, controlled photodissociation reactions enable for creation of atomic and molecular fragments in specific quantum states and use them for researching the selected properties of matter [23, 24, 25, 6, 26]. While the dissociation through the barrier of the potential (tunneling) is well described by an exponential decay [27, 28, 29], the dissociation of the system of coupled excited electronic states should be rather described by other forms of decays. Several different models for these kinds of decays were investigated, such as product decay [30], dephasing [31], and the power-law decay [32, 33, 34].

Our study aims to show the time-dependent descriptions of the excitation and dissociation processes in the polar alkali diatomic molecules and the quantum properties of these reactions in their characteristic time regimes. We propose the femtosecond laser impulse parameters' optimization procedure providing the maximization of the population in the coupled complex of excited electronic states. Dynamics investigations of this system of molecular states allow us, in the case of an association, to establish the optimal time delays for the femtosecond laser impulses enabling the formation of molecules in the deeply bound ground state, as well as present the generally modified power-law decay allowing for the proper description of the dissociation process.

Our considerations are based on an exemplary polar alkaline dimer, which is the NaRb molecule. The sodium rubidium molecular system has been studied both experimentally [35, 36, 37, 38, 39, 40] and theoretically [41, 42, 43, 44]. It is worth underlining that in a recent experiment [45, 46] Guo et al. reported successful production of an ultracold sample of $^{23}Na^{87}$Rb molecules. They used the Feshbach resonance formed by magnetoassociation and populated the lower vibrational levels of the ground state by high-efficiency two-photon Raman processes.

In recent years, in the field of quantum dynamics several numerical methods and their improvements have been introduced, including higher-order split operator methods, the ex-

*Corresponding author at Faculty of Applied Physics and Mathematics, Gdańsk University of Technology, 80-233 Gdańsk, Poland.
Email address: patryk.jasik@pg.edu.pl (P. Jasik)

pansion of the time evolution operator to Chebyshev polynomials [47, 48, 49, 50, 51], or the *semi-global* method [52]. The effective Hamiltonian for describing nuclear kinetics in coupled multiple adiabatic or diabatic electronic states plays a key role in the investigated system. Therefore, in the present study, we apply our newly-developed code [53] to simulate the impulse-driven dynamics of photoassociation of the NaRb dimer that takes the spin-orbit coupling, which varies with the distance between the nuclei, into consideration. The dynamics of multiple coupled electronic states is determined by solutions to the coupled time-dependent Schrödinger equations which also includes an external, classical time-dependent electric field.

In our study, the NaRb dimer is excited from the ground triplet state $1^3\Sigma^+$ to the $1^3\Pi$ state using the femtosecond impulse and the spin-orbit coupling between the $1^3\Pi$ and $2^1\Sigma^+$ states results in the singlet-triplet transition. In the present analysis, we use the lowest electronic states of the NaRb molecule with a rotational quantum state fixed at $J = 0$, appropriate transition dipole moment functions (TDMF), and spin-orbit coupling (SOC) matrix elements. Although accurate experimental potential energy curves and SOCs obtained using deperturbation approach are available in literature, e.g. [39], we use our theoretically derived Born-Oppenheimer potential energy curves (PEC) which were presented in our previous work [43], in order to keep consistency of our calculations (the same set of effective core potentials, core polarization potentials, and basis sets for Na and Rb atoms, as well as the same active space in the configuration interaction method is used for PEC, SOC and TDMF). The impulse is modeled via the classical, time-dependent electric field that interacts with the electronic states via the dipole moments. Since our model includes two excited electronic states, excitations to higher states, including two- and multi-step excitations, are neglected. Such excitations would decrease the overall efficiency of the population transfer to the considered singlet-triplet mixture of excited states.

The femtosecond impulse parameters are optimized to obtain maximum yield in electronic states correlating with the first excited atomic asymptote. We present a map of the optimization space of the impulse parameters and the detailed population statistics. Inspired by [32] we propose a modified power law to describe the population decay.

2. Computation method

The time propagation of a system of coupled time-dependent nuclear Schrödinger equations (TDSE) for multiple electronic states and time-dependent Hamiltonian follows the *semi-global* method [52]. The coupling between the electronic states caused by the electric field is time-dependent. The TDSE has the following form

$$i\hbar\frac{\partial}{\partial t}\begin{pmatrix}\psi_1\\ \psi_2\\ \psi_3\end{pmatrix} = \begin{bmatrix}\hat{\mathbf{H}}_1 & 0 & \hat{\mathbf{V}}_{1,3}\\ 0 & \hat{\mathbf{H}}_2 & \hat{\mathbf{V}}_{2,3}\\ \hat{\mathbf{V}}_{3,1} & \hat{\mathbf{V}}_{3,2} & \hat{\mathbf{H}}_3\end{bmatrix}\begin{pmatrix}\psi_1\\ \psi_2\\ \psi_3\end{pmatrix}, \qquad (1)$$

where the $\hat{\mathbf{H}}_m$ corresponds to the Hamiltonian for the respective electronic state in the Born-Oppenheimer approximation

Table 1: The schematic view of the Hamiltonian matrix of the system used in the calculations. The TDMFs between electronic states μ multiplied by the electric field $E(t)$ are marked with '+'. The lack of coupling between states is marked with '∘'. The spin-orbit coupling is marked with SOC. The PECs are on the matrix diagonal.

	$1^3\Sigma^+$	$2^1\Sigma^+$	$1^3\Pi$
$1^3\Sigma^+$	PEC	∘	+
$2^1\Sigma^+$	∘	PEC	SOC
$1^3\Pi$	+	SOC	PEC

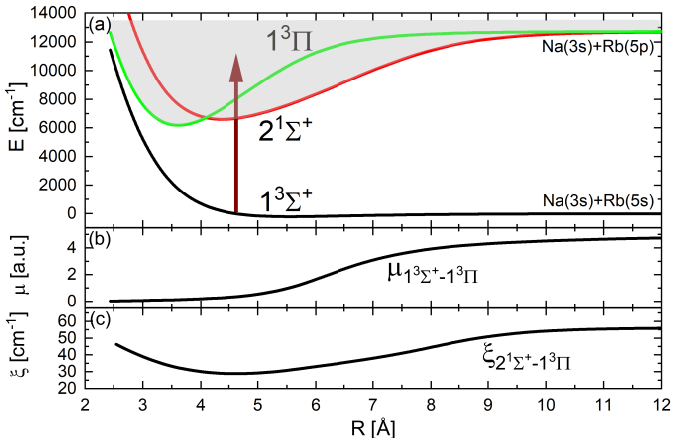

Figure 1: (a) electronic states of the NaRb molecule with a schematic arrow showing the transition imposed by the impulse and a gray area representing excited vibrational states; (b) the transition dipole moment function μ and (c) the spin-orbit coupling ξ. See Tab. 1 for the schematic view of the Hamiltonian in which they are used.

$$\hat{\mathbf{H}}_m = -\frac{\hbar^2}{2M}\nabla^2 + V_m(R) \qquad m = 1, 2, 3 \qquad (2)$$

and $\hat{\mathbf{V}}_{m,n}(t)$ are either (1) the respective transition dipole moment functions μ multiplied[1] by the impulse electric field $E(t)$ or (2) the spin-orbit potential ξ; depending on the nature of the coupling between the two electronic states as follows

$$\begin{aligned}\hat{\mathbf{V}}_{1,3}(R,t) = \hat{\mathbf{V}}_{3,1}(R,t) &= -\mu_{1^3\Sigma^+-1^3\Pi}(R)\,E(t)\\ \hat{\mathbf{V}}_{2,3}(R) \quad = \hat{\mathbf{V}}_{3,2}(R) \quad &= \xi_{2^1\Sigma^+-1^3\Pi}(R).\end{aligned} \qquad (3)$$

The Hamiltonian for three electronic states is summarized in Tab. 1.

The gist of the *semi-global* method [52, 53] is that the evolution operator is expanded, using K terms, in the Krylov space into two parts: (1) the time-dependent part of the Hamiltonian and (2) the Hamiltonian in the middle of the timestep $t + \frac{\Delta t}{2}$, for which the time-dependent part serves as a correction calculated in the M interior sub-timesteps. The calculation of solutions

[1] Following Tannor [27] (page 396) we neglect the vector character of μ because the non-rotating molecule (J=0) is oriented along the propagation direction of the linearly polarised laser field.

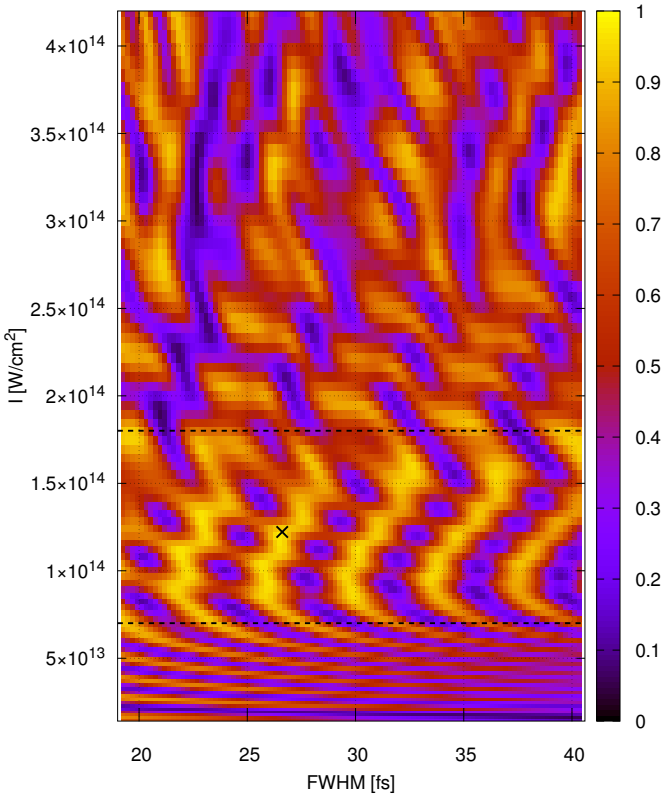

Figure 2: Sum of the population on $2^1\Sigma^+$ and $1^3\Pi$ depending on the FWHM of the laser impulse and its intensity I. The peak population $P_0 = 97.2\%$ at FWHM=26.6 fs, $I = 1.2215 \times 10^{14}$ [W/cm^2] is marked with a cross. The horizontal bands separated by dashed lines are discussed in the text.

for M interior sub-timesteps is iterated several times (usually two to five) within a single global timestep Δt until the solution converges with the requested error tolerance ϵ. Then the calculation moves on to the next timestep.

The *semi-global* method is implemented in C++, thus allowing calculations faster than the original Matlab code [52] and extended with the ability to handle an arbitrary number of electronic states (a feature not present in [52]) such as in Eq. 1. It is then used with the following parameters (which are discussed in detail in [52]): the timestep $\Delta t = 1$ a.u., the number of interior Chebyshev time points $M = 5$ and the number of expansion terms used for the computation of the function of a matrix $K = 7$. The error tolerance is set to $\epsilon = 10^{-10}$. The discretization grid has 6144 points and the absorbing boundary condition (the same as in [52]) is placed at the distance $R_{max} = 70\ a_0$.

3. Results and discussion

Our previously calculated PECs [43], TDMF $\mu_{1^3\Sigma^+-1^3\Pi}$ and SOC $\xi_{2^1\Sigma^+-1^3\Pi}$ along with the schematic transitions are shown in Fig. 1.

As the initial condition, the $v = 20$ eigenfunction of the $1^3\Sigma^+$ state is used, because it is one of the highest populated levels obtained in the experiment [45, 46]. Then the following unchirped impulse is used:

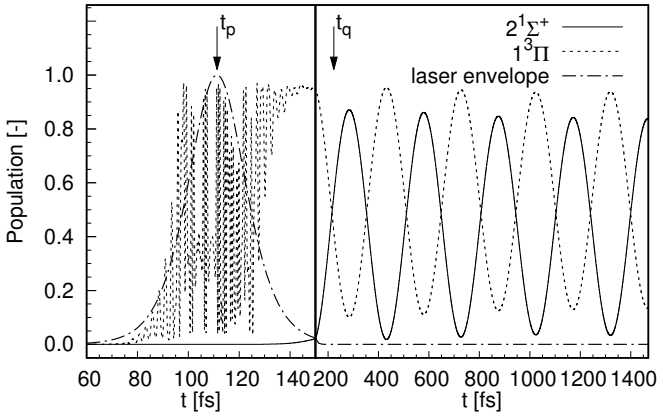

Figure 3: The evolution of the population on the two excited states ($2^1\Sigma^+$, $1^3\Pi$). The impulse FWHM is 26.6 fs, the intensity is 1.2215×10^{14} [W/cm^2] and the wavelength is 1560 nm. The impulse parameters correspond to the peak population found in the scan in Fig. 2. The period of oscillation between the two levels is 296.35 fs. The first peak of $2^1\Sigma^+$ is 172.49 fs after t_p (see Eq. 4). The $t_q = 222.53$ fs (9200 a.u.) marks the end of the laser impulse at which Fig. 2 is shown. In the figure, the first 60 fs, when the impulse is weak and the population is near zero, are not shown for brevity.

$$E(t) = E_o\ \mathrm{sech}^2\left((t - t_p)/\tau_p\right)\cos(\omega t), \qquad (4)$$

where the frequency ω corresponds to a commercially available laser with the wavelength $\lambda = 1560$ nm, the impulse center $t_p = 111.26$ fs (4600 a.u., also marked in Fig. 3 with an arrow), while the maximum intensity $I = \varepsilon_0 c E_0^2/2$ and the full width at half maximum (FWHM) are optimized to maximize the population on the excited state (the FWHM of the impulse equals to $1.76\tau_p$). The laser sech^2 envelope is shown in Fig. 3. The optimization is performed by scanning a range of these two parameters. The optimal FWHM was found to be equal to 26.6 fs and is comparable to the period of vibration motion of the molecule. This requires potential energy curves that decribe electronic states to be accurate in dynamics calculations. The laser intensity scan range extends from 10^{10} to 10^{15} W/cm^2. In our three-states model, an intensity of the order 10^{14} gives the highest population in the upper triplet state. This is the starting point for calculating the population distribution. Despite the limitations of the model of the molecular structure, they provide important physical information about the decay process.

The scan of the sum of the population on two excited states $2^1\Sigma^+$ and $1^3\Pi$ is shown in Fig. 2 at time t_q=222.53 fs (9200 a.u.) marked in Fig. 3 as the end of the laser impulse. We note the existence of three characteristic horizontal bands. The first band occurs for the intensity $I < 0.7 \times 10^{14}$ [W/cm^2]. Here the horizontal lines of the higher population indicate that the FWHM energy spread of the impulse does not affect the population and it mostly depends on the impulse intensity. The second band is in the middle range of I between 0.7×10^{14} and 1.8×10^{14} [W/cm^2]. Here a semi-diagonal pattern emerges where the FWHM energy spread dependence plays a major role. Finally in the third range for $I > 1.8 \times 10^{14}$ [W/cm^2] a chaotic pattern emerges.

Next, using the optimal parameters I and FWHM (marked

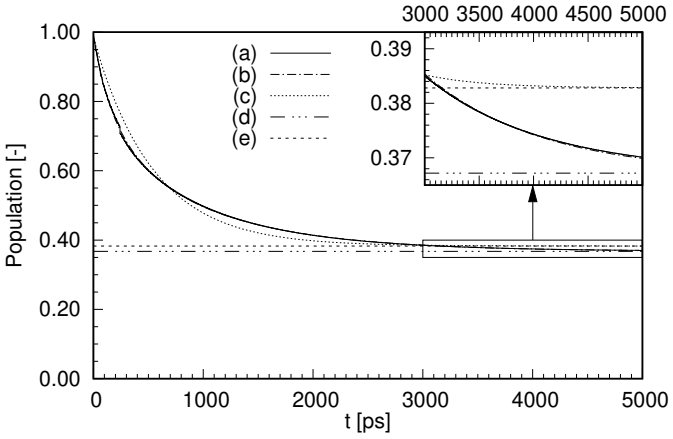

Figure 4: Sum of population on $2^1\Sigma^+$ and $1^3\Pi$ decaying during the first 5000 ps. The decay starts at $t_0 = 10$ ps. (a) numerical result; (b) best fit using the power-law in Eq. 5; (c) best fit using the exponential decay law in Eq. 6; (d) The best fit value of the final population $P_{f,pow}$ in Eq. 5; (e) The best fit value of the final population $P_{f,exp}$ in Eq. 6.

with a cross in Fig. 2) corresponding to the maximum population, the time evolution of the population happens mainly on the excited electronic states. Fig. 3 shows results for obtaining the maximum population found of the $1^3\Pi$ excited state, which is $P_0 = 97.2\%$.

The effect of the spin-orbit coupling is visible in Fig. 3 as the population exchange between electronic states $2^1\Sigma^+$ and $1^3\Pi$. The period of the oscillation between the two states is 296.35 fs. The first maximum on $2^1\Sigma^+$ occurs 172.49 fs after the center of the impulse t_p. In our model, this would be the optimal time delay for the next impulse to dump the molecule from the $2^1\Sigma^+$ state to the absolute ground state using the dumping impulses occurring with a period of 296.35 fs. It means that the peaks of the impulses should correspond to the peaks of the population in the $2^1\Sigma^+$ state.

The population between the electronic states is constantly exchanged due to the spin-orbit coupling. Figure 4 shows the decay of the population within the first nanosecond while the occurrence of spontaneous emission to the ground state is still negligible. The higher frequencies in the wavepacket corresponding to energies that are above the first excited atomic asymptote are undergoing a dissociation. This process is slowed down due to the evolution of the wavepacket on the coupled potential of two excited electronic states. This causes a population decay over a larger timescale and only a fraction of the original population remains at the end, as shown in Fig. 4[2]. As we show below, this is not an exponential decay as in the predissociation process [29]. Instead, it is a distribution of the power law, as it happens by the coincidence of population exchange between two states [32, 54, 55, 56].

Following the idea in [32], that the population decay in the case of two coupled states should follow a power-law decay, we analyze the population decay on the two excited states $2^1\Sigma^+$ and $1^3\Pi$ in our model. The calculated population from Fig. 4 is fitted respectively to the modified power-law decay formula:

$$P(t) = P_0\left(\left(1 - P_{f,pow}\right)\left(\frac{\tau_{pow}}{t + \tau_{pow} - t_0}\right)^{\alpha t+\beta} + P_{f,pow}\right) \qquad (5)$$

and to the exponential decay formula:

$$P(t) = P_0\left(\left(1 - P_{f,exp}\right)\exp\left(-\frac{t - t_0}{\tau_{exp}}\right) + P_{f,exp}\right), \qquad (6)$$

where $P_0 = 97.2\%$ is the initial population on both states, $t_0 = 10$ ps is the start of the decay (when the wavepacket reaches the absorbing potential), τ_{pow}, τ_{exp} are the fitting decay parameters, and $P_{f,pow}$ and $P_{f,exp}$ are the fitting parameters describing the final non-zero population. Additional parameters, α and β, are added to improve the fit, whereas in [32] used a square root in this place. The $(\tau_{pow}/\bullet)$ part of Eq. 5 was modified with respect to [32] with an extra τ_{pow} in the denominator in order to shift the function to the left so that the initial population is not infinite when $t = t_0$ (as is the case in [32]), but instead equals P_0. Also in both equations for decay we used a modification of type: $(1 - P_f) \bullet + P_f$ to allow extra fitting parameters $P_{f,pow}$ and $P_{f,exp}$ for the final non-zero population. It shall be noted that compared to [32] the situation here is also different: both potentials $2^1\Sigma^+$ and $1^3\Pi$ are bonding potentials and neither of them is dissociative (see Fig. 1). Therefore, we use modified power-law decay to fit our numerical results.

The fit results in Fig. 4 are as follows: $\tau_{pow} = 215.86 \pm 0.17$ ps, $P_{f,pow} = 0.3776 \pm 10^{-5}$ (the value on Fig. 4 is $0.3776 \times 97.2\% = 36.7\%$), $\alpha = 2.004 \times 10^{-4} \pm 10^{-7}$, $\beta = 0.6979 \pm 0.0004$ and $\tau_{exp} = 543.0 \pm 0.3$ ps, $P_{f,exp} = 0.3937 \pm 0.0001$ (the value on Fig. 4 is $0.3937 \times 97.2\% = 38.2\%$). For the power law RMSE= 0.0067 and $R^2 = 0.996$, while for the exponential fit RMSE= 0.0185 and $R^2 = 0.972$. The best fit for exponential law produces a nonphysical result because the fitted final population $P_{f,exp}$ (Fig. 4e) has value greater than the steadily decreasing population (a). The fit for the power-law (Fig. 4b) is significantly better, since it almost overlaps the numerical result from the last timestep (Fig. 4a). The final population from the modified power law (Fig. 4d) is $P_{f,pow} \times 97.2\% = 36.7\%$. At 5 ns the calculated population dropped down to 37%. Overall, the modified power law provides a better description of the decay occurring in the spin-orbit-mediated dissociation process.

4. Conclusions

In our study, we show the time evolution on the three coupled potential energy curves of the diatomic alkali metals system – NaRb. The necessary potential energy curves were taken from our earlier ab initio calculations and are presently supplemented with electronic transition dipole moment and spin-orbit coupling between the $2^1\Sigma^+$ and $1^3\Pi$ states. The dynamics of the considered system is driven by a femtosecond impulse. The two parameters describing the impulse, i.e. intensity and FWHM,

[2]Fig. 4 took 6 months to calculate on single thread on processor AMD EPYC 7702P with 3.35 GHz boost clock speed, with discretization grid having 6144 points per electronic level.

are independently optimized, in order to obtain the largest possible population of molecular states correlated with the first excited atomic asymptote. We also identify the period of population oscillation between the two excited states $2^1\Sigma^+$ and $1^3\Pi$.

This allows us to estimate the optimal time delay between the pump and dump impulses, in order to show the possibility of obtaining the NaRb molecule in the singlet ground electronic state. In this approach, the optimal time delay after a pump pulse to dump the molecule to the ground state is 172.49 fs using a pulse with a period of 296.35 fs. We are also examining the combined population decay from the two excited singlet and triplet states. We fit the decay of the population to a modified power law and show that this fit describes this process better than an exponential decay. We emphasize that these results can provide insight into the quantum dynamical processes in diatomic molecules, where time plays a key role. Our approach is possible to apply to even more complex systems where one soft bond (e.g. between two fragments in a molecule) is most important to describe a time-dependent process. We also confirm that impulse control can be applied to the spin-orbit coupled states.

The possible extension of the calculations presented here is to replace the femtosecond excitation with a femtosecond laser impulse with intensity and FWHM commonly used in experiments as well as taking into account the permanent dipole moment and light polarisation. Furthermore, an optimisation of the second femtosecond laser impulse to obtain an ultracold NaRb dimer can be performed. Finally, it would be possible to include higher electric and magnetic transition moments, in order to study extremely high intensities.

All dynamic results are obtained from our new computer code which uses a *semi-global* method to expand the time evolution operator. The method is improved to work with multiple electronic states and time-dependent couplings. It can be a valuable tool for studying quantum dynamics and planning future experiments.

Author Information

Corresponding Author
* E-mail: patryk.jasik@pg.edu.pl

ORCID
Janek Kozicki: 0000-0002-8427-7263
Patryk Jasik: 0000-0002-6601-0506
Tymon Kilich: 0000-0001-6831-694X
Józef E. Sienkiewicz: 0000-0002-1149-3846

Conflicts of interest
There are no conflicts of interest to declare

Data availability

The data that support the findings of this study are publicly available in the Bridge of Knowledge Open Data Repository, https://doi.org/10.34808/kkhq-s579.

Acknowledgements

We acknowledge the partial support by the Polish Ministry of Education and Science, COST action CA18222 “Attosecond Chemistry”, and COST action CA21101 “Confined Molecular Systems: From a New Generation of Materials to the Stars”. Calculations have been carried out using resources provided by the Centre of Informatics Tricity Academic Supercomputer & Network and Wroclaw Centre for Networking and Supercomputing.

References

[1] A. H. Zewail, Femtochemistry: Atomic-scale dynamics of the chemical bond, The Journal of Physical Chemistry A 104 (24) (2000) 5660–5694. doi:10.1021/jp001460h.
URL http://dx.doi.org/10.1021/jp001460h

[2] B. Zhao, S. Han, C. L. Malbon, U. Manthe, D. R. Yarkony, H. Guo, Full-dimensional quantum stereodynamics of the non-adiabatic quenching of $OH(A^2\Sigma^+)$ by H_2, Nature Chemistry 13 (9) (2021) 909–915. doi:10.1038/s41557-021-00730-1.
URL https://doi.org/10.1038/s41557-021-00730-1

[3] K.-J. Yuan, C.-C. Shu, D. Dong, A. D. Bandrauk, Attosecond dynamics of molecular electronic ring currents, The Journal of Physical Chemistry Letters 8 (10) (2017) 2229–2235. doi:10.1021/acs.jpclett.7b00877.
URL http://dx.doi.org/10.1021/acs.jpclett.7b00877

[4] P. J. Ollitrault, A. Miessen, I. Tavernelli, Molecular quantum dynamics: A quantum computing perspective, Accounts of Chemical Research 54 (23) (2021) 4229–4238. doi:10.1021/acs.accounts.1c00514.
URL https://doi.org/10.1021/acs.accounts.1c00514

[5] S. Jahangiri, J. M. Arrazola, A. Delgado, Quantum algorithm for simulating single-molecule electron transport, The Journal of Physical Chemistry Letters 12 (4) (2021) 1256–1261. doi:10.1021/acs.jpclett.0c03724.
URL http://dx.doi.org/10.1021/acs.jpclett.0c03724

[6] Z. Wei, J. Li, S. T. See, Z.-H. Loh, Spin–orbit state-selective C–I dissociation dynamics of the CH_3I^+ $\tilde{X}$ electronic state induced by intense few-cycle laser fields, The Journal of Physical Chemistry Letters 8 (24) (2017) 6067–6072. doi:10.1021/acs.jpclett.7b03022.
URL http://dx.doi.org/10.1021/acs.jpclett.7b03022

[7] T. Bai, Z. Qin, L. Liu, Spin-forbidden electronic transition properties of MgO, Journal of Quantitative Spectroscopy and Radiative Transfer 251 (2020) 107086. doi:https://doi.org/10.1016/j.jqsrt.2020.107086.
URL https://www.sciencedirect.com/science/article/pii/S0022407320301850

[8] I. S. Vinklárek, J. Suchan, J. Rakovský, K. Moriová, V. Poterya, P. Slavíček, M. Fárník, Energy partitioning and spin–orbit effects in the photodissociation of higher chloroalkanes, Physical Chemistry Chemical Physics 23 (26) (2021) 14340–14351. doi:10.1039/d1cp01371h.
URL http://dx.doi.org/10.1039/d1cp01371h

[9] Y. Chang, Y. Yu, F. An, Z. Luo, D. Quan, X. Zhang, X. Hu, Q. Li, J. Yang, Z. Chen, L. Che, W. Zhang, G. Wu, D. Xie, M. N. R. Ashfold, K. Yuan, X. Yang, Three body photodissociation of the water molecule and its implications for prebiotic oxygen production, Nature Communications 12 (1) (Apr 2021). doi:10.1038/s41467-021-22824-7.
URL http://dx.doi.org/10.1038/s41467-021-22824-7

[10] Y. Zhao, Z. Luo, Y. Chang, Y. Wu, S.-e. Zhang, Z. Li, H. Ding, G. Wu, J. S. Campbell, C. S. Hansen, S. W. Crane, C. M. Western, M. N. R. Ashfold, K. Yuan, X. Yang, Rotational and nuclear-spin level dependent photodissociation dynamics of H_2S, Nature Communications 12 (1) (Jul 2021). doi:10.1038/s41467-021-24782-6.
URL http://dx.doi.org/10.1038/s41467-021-24782-6

[11] M. L. Murillo-Sánchez, G. Reitsma, S. M. Poullain, P. Fernández-Milán, J. González-Vázquez, R. de Nalda, F. Martín, M. J. J. Vrakking, O. Kornilov, L. Bañares, Femtosecond XUV–IR induced photodynamics in the methyl iodide cation, New Journal of Physics 23 (7) (2021) 073023.

doi:10.1088/1367-2630/ac0c9b.
URL http://dx.doi.org/10.1088/1367-2630/ac0c9b
[12] C. P. Koch, M. Shapiro, Coherent control of ultracold photoassociation, Chemical Reviews 112 (9) (2012) 4928–4948. doi:10.1021/cr2003882.
URL http://dx.doi.org/10.1021/cr2003882
[13] J. Ulmanis, J. Deiglmayr, M. Repp, R. Wester, M. Weidemüller, Ultracold molecules formed by photoassociation: Heteronuclear dimers, inelastic collisions, and interactions with ultrashort laser pulses, Chemical Reviews 112 (9) (2012) 4890–4927. doi:10.1021/cr300215h.
URL http://dx.doi.org/10.1021/cr300215h
[14] J. L. Carini, S. Kallush, R. Kosloff, P. L. Gould, Efficient formation of ultracold molecules with chirped nanosecond pulses, The Journal of Physical Chemistry A 120 (19) (2015) 3032–3041. doi:10.1021/acs.jpca.5b10088.
URL http://dx.doi.org/10.1021/acs.jpca.5b10088
[15] M. Tomza, K. Jachymski, R. Gerritsma, A. Negretti, T. Calarco, Z. Idziaszek, P. S. Julienne, Cold hybrid ion-atom systems, Reviews of Modern Physics 91 (3) (Jul 2019). doi:10.1103/revmodphys.91.035001.
URL http://dx.doi.org/10.1103/RevModPhys.91.035001
[16] X. Wang, W. Liu, J. Wu, V. B. Sovkov, J. Ma, P. Li, L. Xiao, S. Jia, Saturation of photoassociation in NaCs dark magneto-optical trap, Journal of Quantitative Spectroscopy and Radiative Transfer 240 (2020) 106678. doi:https://doi.org/10.1016/j.jqsrt.2019.106678.
URL https://www.sciencedirect.com/science/article/pii/S0022407319304315
[17] M. Weyland, S. Szigeti, R. Hobbs, P. Ruksasakchai, L. Sanchez, M. Andersen, Pair correlations and photoassociation dynamics of two atoms in an optical tweezer, Physical Review Letters 126 (8) (Feb 2021). doi:10.1103/physrevlett.126.083401.
URL http://dx.doi.org/10.1103/PhysRevLett.126.083401
[18] D. Borsalino, B. Londoño-Florèz, R. Vexiau, O. Dulieu, N. Bouloufa-Maafa, E. Luc-Koenig, Efficient optical schemes to create ultracold KRb molecules in their rovibronic ground state, Physical Review A 90 (3) (Sep 2014). doi:10.1103/physreva.90.033413.
URL http://dx.doi.org/10.1103/PhysRevA.90.033413
[19] D. Borsalino, R. Vexiau, M. Aymar, E. Luc-Koenig, O. Dulieu, N. Bouloufa-Maafa, Prospects for the formation of ultracold polar ground state KCs molecules via an optical process, Journal of Physics B: Atomic, Molecular and Optical Physics 49 (5) (2016) 055301. doi:10.1088/0953-4075/49/5/055301.
URL http://dx.doi.org/10.1088/0953-4075/49/5/055301
[20] N. Balakrishnan, Perspective: Ultracold molecules and the dawn of cold controlled chemistry, The Journal of Chemical Physics 145 (15) (2016) 150901. doi:10.1063/1.4964096.
URL http://dx.doi.org/10.1063/1.4964096
[21] A. Devolder, M. Desouter-Lecomte, O. Atabek, E. Luc-Koenig, O. Dulieu, Laser control of ultracold molecule formation: The case of RbSr, Phys. Rev. A 103 (2021) 033301. doi:10.1103/PhysRevA.103.033301.
URL https://link.aps.org/doi/10.1103/PhysRevA.103.033301
[22] K. H. Leung, E. Tiberi, B. Iritani, I. Majewska, R. Moszynski, T. Zelevinsky, Ultracold $^{88}Sr_2$ molecules in the absolute ground state, New Journal of Physics 23 (11) (2021) 115002. doi:10.1088/1367-2630/ac2dac.
URL http://dx.doi.org/10.1088/1367-2630/ac2dac
[23] A. B. Alekseyev, H.-P. Liebermann, R. J. Buenker, N. Balakrishnan, H. R. Sadeghpour, S. T. Cornett, M. J. Cavagnero, Spin–orbit effects in photodissociation of sodium iodide, The Journal of Chemical Physics 113 (4) (2000) 1514–1523. doi:10.1063/1.481938.
URL http://dx.doi.org/10.1063/1.481938
[24] E. Kokkonen, T. Löytynoja, K. Jänkälä, J. A. Kettunen, S. Heinäsmäki, A. Karpenko, M. Huttula, Spin–orbit interaction mediated molecular dissociation, The Journal of Chemical Physics 140 (18) (2014) 184304. doi:10.1063/1.4873718.
URL http://dx.doi.org/10.1063/1.4873718
[25] M. McDonald, B. H. McGuyer, F. Apfelbeck, C. H. Lee, I. Majewska, R. Moszynski, T. Zelevinsky, Photodissociation of ultracold diatomic strontium molecules with quantum state control, Nature 535 (7610) (2016) 122–126. doi:10.1038/nature18314.
URL http://dx.doi.org/10.1038/nature18314
[26] A. Tóth, A. Csehi, G. J. Halász, A. Vibók, Control of photodissociation with the dynamic stark effect induced by thz pulses, Phys. Rev. Research 2 (2020) 013338. doi:10.1103/PhysRevResearch.2.013338.
URL https://link.aps.org/doi/10.1103/PhysRevResearch.2.013338
[27] D. J. Tannor, Introduction to quantum mechanics: a time-dependent perspective, University Science Books, Sausalito, 2007.
[28] H. Schmidt, J. von Vangerow, F. Stienkemeier, A. S. Bogomolov, A. V. Baklanov, D. M. Reich, W. Skomorowski, C. P. Koch, M. Mudrich, Predissociation dynamics of lithium iodide, The Journal of Chemical Physics 142 (4) (2015) 044303. doi:10.1063/1.4906512.
URL http://dx.doi.org/10.1063/1.4906512
[29] P. Jasik, J. Kozicki, T. Kilich, J. E. Sienkiewicz, N. E. Henriksen, Electronic structure and rovibrational predissociation of the $2^1\Pi$ state in KLi, Physical Chemistry Chemical Physics 20 (27) (2018) 18663–18670. doi:10.1039/c8cp02551g.
URL http://dx.doi.org/10.1039/c8cp02551g
[30] J. Kong, X. Shang, W. Zheng, X. Chen, D. Tu, M. Wang, J. Song, J. Qu, Revisiting the luminescence decay kinetics of energy transfer upconversion, The Journal of Physical Chemistry Letters 11 (9) (2020) 3672–3680. doi:10.1021/acs.jpclett.0c00619.
URL http://dx.doi.org/10.1021/acs.jpclett.0c00619
[31] M. Gruebele, Intramolecular vibrational dephasing obeys a power law at intermediate times, Proceedings of the National Academy of Sciences 95 (11) (1998) 5965–5970. doi:10.1073/pnas.95.11.5965.
URL http://dx.doi.org/10.1073/pnas.95.11.5965
[32] Y. Mizuno, K. Hukushima, Power-law decay in the nonadiabatic photodissociation dynamics of alkali halides due to quantum wavepacket interference, The Journal of Chemical Physics 149 (17) (2018) 174313. doi:10.1063/1.5048957.
URL http://dx.doi.org/10.1063/1.5048957
[33] J. K. Utterback, J. L. Ruzicka, H. Hamby, J. D. Eaves, G. Dukovic, Temperature-dependent transient absorption spectroscopy elucidates trapped-hole dynamics in CdS and CdSe nanorods, The Journal of Physical Chemistry Letters 10 (11) (2019) 2782–2787. doi:10.1021/acs.jpclett.9b00764.
URL http://dx.doi.org/10.1021/acs.jpclett.9b00764
[34] Y. Dong, L. Dong, M. Gong, H. Pu, Dynamical phases in quenched spin–orbit-coupled degenerate fermi gas, Nature Communications 6 (1) (Jan 2015). doi:10.1038/ncomms7103.
URL http://dx.doi.org/10.1038/ncomms7103
[35] M. Tamanis, R. Ferber, A. Zaitsevskii, E. A. Pazyuk, A. V. Stolyarov, H. Chen, J. Qi, H. Wang, W. C. Stwalley, High resolution spectroscopy and channel-coupling treatment of the $A^1\Sigma^+ - b^3\Pi$ complex of NaRb, The Journal of Chemical Physics 117 (17) (2002) 7980–7988. doi:10.1063/1.1505442.
URL http://dx.doi.org/10.1063/1.1505442
[36] O. Docenko, M. Tamanis, R. Ferber, A. Pashov, H. Knöckel, E. Tiemann, Potential of the ground state of narb, Phys. Rev. A 69 (2004) 042503. doi:10.1103/PhysRevA.69.042503.
URL https://link.aps.org/doi/10.1103/PhysRevA.69.042503
[37] A. Jarmola, M. Tamanis, R. Ferber, E. Pazyuk, A. Stolyarov, LIF intensity distribution as a deperturbation tool: application to the fully-mixed $A^1\Sigma^+$–$b^3\Pi$ complex of narb, Journal of Quantitative Spectroscopy and Radiative Transfer 95 (2) (2005) 165–174. doi:https://doi.org/10.1016/j.jqsrt.2004.10.003.
URL https://www.sciencedirect.com/science/article/pii/S0022407304004509
[38] A. Pashov, W. Jastrzebski, P. Kortyka, P. Kowalczyk, Experimental long range potential of the $B^1\Pi$ state in NaRb, The Journal of Chemical Physics 124 (20) (2006) 204308. doi:10.1063/1.2198199.
URL http://dx.doi.org/10.1063/1.2198199
[39] O. Docenko, M. Tamanis, R. Ferber, E. A. Pazyuk, A. Zaitsevskii, A. V. Stolyarov, A. Pashov, H. Knöckel, E. Tiemann, Deperturbation treatment of the $a\,^1\Sigma^+ - -b\,^3\Pi$ complex of NaRb and prospects for ultracold molecule formation in $x\,^1\Sigma^+(v = 0; j = 0)$, Phys. Rev. A 75 (2007) 042503. doi:10.1103/PhysRevA.75.042503.
URL https://link.aps.org/doi/10.1103/PhysRevA.75.042503
[40] Z. Guo, F. Jia, B. Zhu, L. Li, J. M. Hutson, D. Wang, Improved

characterization of feshbach resonances and interaction potentials between ^{23}Na and ^{87}Rb atoms, Phys. Rev. A 105 (2022) 023313. doi:10.1103/PhysRevA.105.023313.
URL https://link.aps.org/doi/10.1103/PhysRevA.105.023313

[41] M. Korek, A. Allouche, M. Kobeissi, A. Chaalan, M. Dagher, K. Fakherddin, M. Aubert-Frécon, Theoretical study of the electronic structure of the LiRb and NaRb molecules, Chemical Physics 256 (1) (2000) 1–6. doi:10.1016/s0301-0104(00)00061-6.
URL http://dx.doi.org/10.1016/S0301-0104(00)00061-6

[42] M. Chaieb, H. Habli, L. Mejrissi, B. Oujia, F. X. Gadéa, Ab initio spectroscopic study for the NaRb molecule in ground and excited states, International Journal of Quantum Chemistry 114 (11) (2014) 731–747. doi:10.1002/qua.24664.
URL http://dx.doi.org/10.1002/qua.24664

[43] M. Wiatr, P. Jasik, J. E. Sienkiewicz, The adiabatic potentials of low-lying electronic states of the NaRb molecule, Physica Scripta 90 (5) (2015) 054012. doi:10.1088/0031-8949/90/5/054012.
URL http://dx.doi.org/10.1088/0031-8949/90/5/054012

[44] M. Wiatr, P. Jasik, T. Kilich, J. E. Sienkiewicz, H. Stoll, Quasirelativistic potential energy curves and transition dipole moments of NaRb, Chemical Physics 500 (2018) 80–87. doi:10.1016/j.chemphys.2017.10.005.
URL http://dx.doi.org/10.1016/j.chemphys.2017.10.005

[45] M. Guo, B. Zhu, B. Lu, X. Ye, F. Wang, R. Vexiau, N. Bouloufa-Maafa, G. Quéméner, O. Dulieu, D. Wang, Creation of an ultracold gas of ground-state dipolar ^{23}Na^{87}rb molecules, Physical Review Letters 116 (20) (May 2016). doi:10.1103/physrevlett.116.205303.
URL http://dx.doi.org/10.1103/PhysRevLett.116.205303

[46] M. Guo, R. Vexiau, B. Zhu, B. Lu, N. Bouloufa-Maafa, O. Dulieu, D. Wang, High-resolution molecular spectroscopy for producing ultracold absolute-ground-state ^{23}Na^{87}Rb molecules, Physical Review A 96 (5) (Nov 2017). doi:10.1103/physreva.96.052505.
URL http://dx.doi.org/10.1103/PhysRevA.96.052505

[47] W. Van Dijk, Efficient explicit numerical solutions of the time-dependent schrödinger equation, Physical Review E 105 (2) (2022). doi:10.1103/PhysRevE.105.025303.

[48] M. B. Soley, P. Bergold, A. A. Gorodetsky, V. S. Batista, Functional tensor-train chebyshev method for multidimensional quantum dynamics simulations, Journal of Chemical Theory and Computation 18 (1) (2022) 25 – 36. doi:10.1021/acs.jctc.1c00941.

[49] H. Tal-Ezer, R. Kosloff, An accurate and efficient scheme for propagating the time dependent schrödinger equation, The Journal of Chemical Physics 81 (9) (1984) 3967–3971. doi:10.1063/1.448136.
URL http://dx.doi.org/10.1063/1.448136

[50] R. Kosloff, Quantum molecular dynamics on grids, Department of Physical Chemistry and the Fritz Haber Research Center, 1997.
URL https://scholars.huji.ac.il/sites/default/files/ronniekosloff/files/wayat.pdf

[51] H. Tal-Ezer, R. Kosloff, I. Schaefer, New, highly accurate propagator for the linear and nonlinear schrödinger equation, Journal of Scientific Computing 53 (1) (2012) 211–221. doi:10.1007/s10915-012-9583-x.
URL http://dx.doi.org/10.1007/s10915-012-9583-x

[52] I. Schaefer, H. Tal-Ezer, R. Kosloff, Semi-global approach for propagation of the time-dependent schrödinger equation for time-dependent and nonlinear problems, Journal of Computational Physics 343 (2017) 368–413. doi:10.1016/j.jcp.2017.04.017.
URL http://dx.doi.org/10.1016/j.jcp.2017.04.017

[53] J. Kozicki, Very accurate time propagation of coupled Schrödinger equations for femto- and attosecond physics and chemistry, with C++ source code, Comput. Phys. Commun. submitted (2022).

[54] K. B. Møller, N. E. Henriksen, A. H. Zewail, On the role of coherence in the transition from kinetics to dynamics: Theory and application to femtosecond unimolecular reactions, The Journal of Chemical Physics 113 (23) (2000) 10477–10485. doi:10.1063/1.1323729.
URL http://dx.doi.org/10.1063/1.1323729

[55] M. Shapiro, A uniform theory of preparation, dissociation, and product formation in the decay of overlapping resonances, The Journal of Physical Chemistry A 102 (47) (1998) 9570–9576. doi:10.1021/jp982182d.
URL http://dx.doi.org/10.1021/jp982182d

[56] V. Brems, M. Desouter-Lecomte, Memory kernels and effective hamiltonians from time-dependent methods. ii. vibrational predissociation, The Journal of Chemical Physics 116 (19) (2002) 8318. doi:10.1063/1.1467053.
URL http://dx.doi.org/10.1063/1.1467053